Electron beam density study using a portable slit imaging system at the Shanghai Electron Beam Ion Trap*

Yang Yang(杨 洋)[a)b)], Lu Di(路 迪)[a)b)], Fu Yun-Qing(傅云清)[a)b)], Yao Ke(姚 科)[a)b)], Chen Wei-Dong(陈卫东)[a)b)], Xiao Jun(肖 君)[a)b)], Geng Zhi-Xian(耿志贤)[a)b)], Roger Hutton[a)b)], and Zou Ya-Ming(邹亚明)[a)b)†]

[a)] *The Key Laboratory of Applied Ion Beam Physics of Ministry of Education, Shanghai* 200433, *China*

[b)] *Shanghai Electron Beam Ion Trap Laboratory, Institute of Modern Physics, Fudan University, Shanghai* 200433, *China*

(Received 12 January 2011; revised manuscript received 1 March 2011)

In this work, a portable slit imaging system is developed to study both the electron beam diameter and the profile of the newly developed Shanghai Electron Beam Ion Trap (Shanghai EBIT). Images are detected by a charge coupled device (CCD) sensitive to both X rays and longer wavelength photons (up to visible). Large scale ray tracings were conducted for correcting the image broadening effects caused by the finite slit width and the finite width of the CCD pixels. A numerical de-convolution method was developed to analyse and reconstruct the electron beam density distribution in the EBIT. As an example of the measured beam diameter and current density, the FWHM (full width at half maximum) diameter of the electron beam at 81 keV and 120 mA is found to be 76.2 μm and the density 2.00×10^3 A·cm^{-2}, under a magnetic field of 3 T, including all corrections.

Keywords: electron beam density, slit imaging, de-convolution

PACS: 07.05.Pj, 07.05.Rm **DOI:** 10.1088/1674-1056/20/8/080701

1. Introduction

Electron beam ion traps (EBITs) have undergone rapid development over the past two decades, as evidenced from the proceedings of a conference marking 20 years of EBIT spectroscopy.[1] As a new and efficient ion and light source for highly charged ion physics, these devices have been widely equipped for spectroscopic studies of highly charged ions, as well as studies of hot plasma physics. In an EBIT facility, the electron beam emitted by the electron gun will be accelerated and guided to the central trap where it will interact with the trapped ions. By compressing the electron beam using a pair of Helmholtz coils,[2] the diameter of the beam in the centre trap area can be reduced to around 1/30 of its original size. In this case the density of the beam will increase by a factor of 10^3 and lead to useful increases in the rates of processes such as ionization, excitation and recombination. Hence the density of the electron beam plays a crucial role in the usefulness of an EBIT.

Some work has previously been done to study the electron beam and ion cloud diameters in EBITs.[3−7] In Ref. [3], the determination of the electron beam diameter at the Livermore EBIT was done using an imaging system employing a gas-filled position sensitive proportional counter for photon detection. In their work the slit was mounted very close to the electron beam, which is not possible for many EBITs. However, by doing so, they were able to use a high magnification. This in turn permitted good image resolution even though they used a proportional counter, which has relatively low spatial resolution. Hence accurate measurements of the electron beam diameter were possible. There was also an earlier measurement at the Livermore EBIT of the beam radius at a single electron beam energy and current.[4] The image resolution and the statistic error were not very satisfactory in that work. In Ref. [5] a visible lens system was used, again at the Livermore EBIT, and visible images of EBIT ion clouds were measured. In that work three different cases were studied: 1) open trap with-

*Project supported by the National Natural Science Foundation of China (Grant No. 11074049), the Chinese National Fusion Project for ITER (Grant No. 2009GB106001), and the Shanghai Leading Academic Discipline Project, China (Grant No. B107).

†Corresponding author. E-mail: zouym@fudan.edu.cn

out gas injection, 2) open trap with gas injection, and 3) closed trap with gas injection. Their results showed that without gas injection there was no detectable visible light. However the introduction of a gas jet showed an obvious enlargement in the image size in the region where the jet crossed the electron beam. This was explained as being caused by the longer lifetimes of the excited neutral and atoms and low charge ions in the crossing region. Their results showed that the diameter of the visible images of the ion cloud could be much larger than that of the electron beam. Further studies of visible images of different charge state ion clouds were done by the NIST EBIT group, using an optical lens system[6] and narrow band filters. They also studied the influence of trap voltage on the width of the ion cloud. In Ref. [7], the spatial distribution and the photon energy of the X-ray radiation from the centre drift tube of an EBIT were measured with a spherically bent quartz crystal and X-ray sensitive change coupled device (CCD). This system made it possible to record a two-dimensional image of the electron beam at the same time as studying the X-ray spectrum of the ion cloud.

In all the work mentioned above, the images of ion clouds in EBITs were formed by the photons from de-excitation of ions excited by the electron beam rather than from the electron beam itself. As discussed in Refs. [4] and [5], visible radiation is mostly from forbidden transitions from metastable states and the longer lifetimes of the metastable states allow the ions to travel further away from the electron beam before de-excitation. Hence the size of the visible images of the ion clouds is usually much larger than that of the electron beam. While X-ray radiation is mostly from allowed transition, where the lifetimes are much shorter, and the ions are not able to move far from the electron beam before de-excitation. Hence X-ray images of the ion cloud in an EBIT should be a better approximation to the size of the electron beam. As stated above we choose to work in the X-ray region of the spectrum. In the work presented here we use a charge coupled device (CCD) sensitive to both X rays and longer wavelength photons, up to the visible range, to acquire images of the electron beam. The images were formed by a 30-μm wide slit acting as a pinhole camera. With this arrangement, we could image the object, i.e. electron beam, in the direction perpendicular to the slit, while an average is recorded along the slit direction. The object in our case was fairly uniform in the region where our slit camera was viewing and hence very suited for this geometry. The high spatial resolution of the particular CCD chip meant that good imaging could be achieved even with low magnification, approximately 1:1 imaging. This means that the object distance (distance from the electron beam to the slit) can be quite large. This made it possible to build a portable X-ray slit imaging system, in which the object distance is much longer than that in a built-in slit/pinhole imaging system used for studying the ion clouds/electron beams in EBITs. As a result, we needed to develop careful analysis tools to infer the desired quantities. Based on a detailed analysis of the recorded images, taking into account the finite slit size, finite CCD pixel size, etc., we could re-construct accurate images of the electron beam. These methods will be discussed in the following text.

2. Experiment

The slit assembly was installed in the centre of a vacuum flange and was calibrated to keep the slit parallel to the electron beam, as shown schematically in Fig. 1. The slit was made from two 20-mm long tungsten blades, with very dull edge, spaced 30 μm apart. A relatively large image distance (the distance between the slit and CCD surface) would lead to a higher magnification of the image system. However, the geometry of the Shanghai EBIT limited the object distance and the weak intensity property of EBIT light source restricted the total distance. So the final compromised object and image distance in our system were 594 mm and 502 mm, respectively, leading to a magnification smaller than a unit, which is 0.845. A CCD of Andor DO436, with (2048 × 2048) 13.5-μm square pixels, was mounted in the image plane for detection. The lower 2/3 surface of the CCD chip was covered with a 60-μm-thick Be window during the experiments. With such an arrangement it was possible for us to compare the images both from only X rays and from all CCD sensitive photons from the EBIT. Figure 2 shows the image of the electron beam of 81 keV and 80 mA, under a 3-T magnetic field, in the trap area recorded using the slit imaging system. In Fig. 2, the image below the horizontal arrow is formed purely by X rays, the upper part is formed by all CCD sensitive photons. The image above the horizontal arrow shows a clear increase in photon intensity and a slight increase in image width.

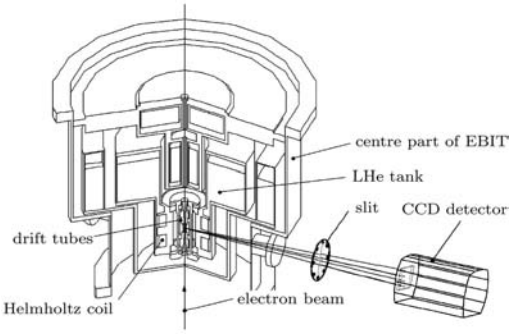

Fig. 1. A schematic diagram of the slit imaging system.

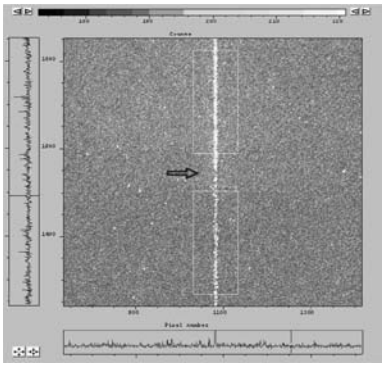

Fig. 2. Part of an image of the electron beam taken using the slit imaging system, with the electron beam energy being 81 keV, the current 80 mA and the magnetic field 3 T and the arrow marking the edge of the Be window.

Gas injection was not used in this work, as it could possibly distort the ion cloud.[5] The ions in the trap came mostly from sputtering process at the cathode of the electron gun and were mainly barium and tungsten. In this work, electron beam densities were studied under the following conditions: 81 keV with currents of 80 mA, 100 mA, and 120 mA; 50 keV with currents of 80 mA, 100 mA, and 113 mA; 20 keV with currents of 60 mA and 80 mA; and finally 100 keV with a current of 100 mA. In all the measurements, the axial trapping voltage was set at 200 V.

3. Data analysis

As each image is averaged along the electron beam (vertical) direction the statistical quality of the data can be increased by binning the data in the vertical direction. The results of the data binning of the two areas in Fig. 2 are shown in Figs. 3(a) and 3(b).

The intensity distribution was then fitted to a Gaussian function of the form

$$\varphi(x) = \varphi_0 + \frac{A}{\sigma\sqrt{2\pi}} \exp\left[-\frac{(x-\mu)^2}{2\sigma^2}\right]. \qquad (1)$$

Here, σ is related to the width of the electron beam image FWHM and FWHM $= 2\sqrt{2\ln 2}\,\sigma$; μ represents the central position of the beam image. The solid lines in Figs. 3(a) and 3(b) are the obtained Gaussian fits. The fitted values of σ are 2.252 pixels and 2.334 pixels which are equivalent to 30.40 μm and 32.00 μm for the data shown in Figs. 3(a) and 3(b) respectively. For the reason discussed in the introduction part, further data analysis was done only for the pure X-ray parts of the recorded images.

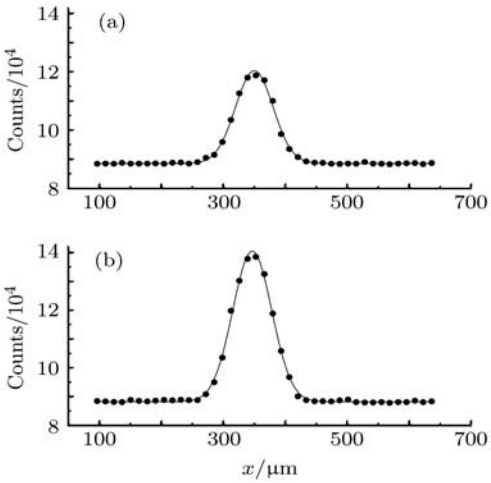

Fig. 3. (a) Intensity distribution across the horizontal axis from the part of the image subject only to X-ray exposure (see Fig. 2) and (b) all photons seen by the CCD, with solid lines representing the results of Gaussian fits.

The width of the slit used in this work is not insignificant with respect to the expected width of the electron beam, hence a de-convolution process is necessary. If we consider an object as a geometrical line parallel to the silt, the intensity $I_{\rm img}$ of its image at the position P in the image plane is inversely proportional to $(D^2 + x^2)$ as shown in Fig. 4, where D is the distance between the object and the image plane and x is the distance to the image centre in the image plane. When the distance D is very large compared with the slit width, the image intensity distribution tends towards a flat top shape.

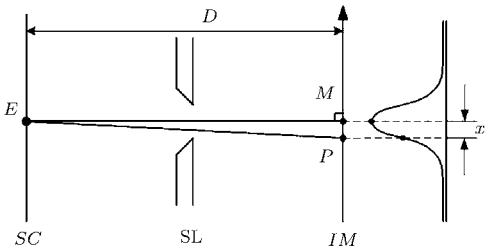

Fig. 4. An illustration of the top view of the slit imaging system with a geometrical line object. The object is marked as point E on the object plane SC. SL is the silt. The distance between the point P and the image centre M on the image plane IM is x.

However, the real object, the electron beam, is not a line and it is usually described by a Gaussian distribution[3,4] across the axis vertical to it. The image could be a convolution of a Gaussian and a flat top distribution. Hence to obtain a reliable profile for the object (the electron beam), it is necessary to deconvolute the flat-top slit function from the recorded image data. This would require an integral over a finite interval of a Gaussian as a part of the algebraic de-convolution process. Such a solution is difficult to obtain, so we developed a numerical scheme based on large scale ray tracing. The numerical scheme is described below.

As shown in Fig. 5 the mid-point M on the image plane, IM, can receive photons from the area between E_1 and E_2 on the object plane, SC. So the intensity at this point should be the integration of the light intensity emitted from the area between E_1 and E_2. Because point M is the midpoint of the Gaussian distribution of the image, half of its intensity should be the value of the "half maximum". Next, a new point on the plane IM is selected and a similar calculation is then applied to this new point using the same method of integration but for a different area on the plane SC, i.e. E_1' to E_2'. Using an iterative computational method it is possible to find a point whose value is equal to the value of the "half maximum" within a given tolerance. This point is marked as $P_{\rm FWHM}$ in the IM plane as shown in Fig. 5. Then, twice the distance between point M and $P_{\rm FWHM}$ is the FWHM of the intensity distribution of the image. Using this method the FWHM of the image can be obtained if the distribution function of the object is known. In addition, if we know the distribution function of the image, which is true, we can obtain the FWHM of the object. We have carried out a large scale ray tracing according to the method described above and obtained the full profile of the image after convolution with the slit system. The profile can be well represented by a Gaussian distribution function as shown in Fig. 6.

Then we assume a Gaussian distribution FWHM of the object and simulate the convolution process to obtain a Gaussian FWHM for the image. We compare the obtained image FWHM with the experimental data. If they are not equal, the assumed object FWHM is varied and the process is repeated. Via iterative computation, an object (electron beam) FWHM is obtained under the tolerance that its image FWHM is equal to the experimental value taken from the CCD image.

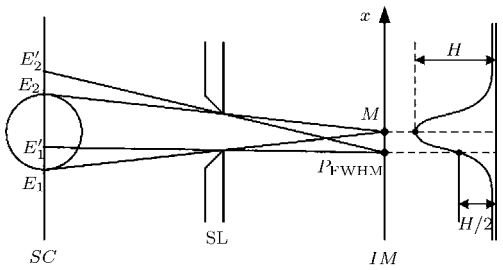

Fig. 5. An illustration of the imaging with a nongeometrical line object, where the notations of the object plane, slit, imaging plane and the image centre are the same as those in Fig. 4.

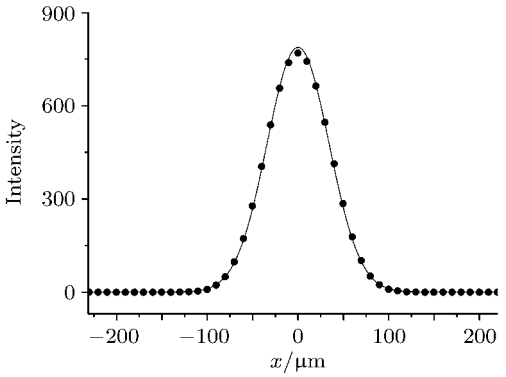

Fig. 6. A full profile of the image from the ray tracing after convolution. The solid circles represent the data points obtained from the simulation and the solid line denotes the fitting result of these data points using a Gaussian distribution function.

So far we have used a one-dimensional Gaussian function to represent the electron beam intensity. However, a two-dimensional distribution function would be more reasonable for describing the sources. Here we assume a two-dimensional Gaussian distribution. For an optically thin plasma, or ion cloud as is the case in an EBIT, it is acceptable to project this distribution onto the plane facing to the slit, i.e. the object plane, and the distribution after projection is still a Gaussian with the same FWHM. This means that the FWHM is not affected by such a projection.

Gaussian functions have already been accepted[3,4] for the electron beam radial distribution in an EBIT. The good fitting results of the image intensity distributions in this work, using Gaussian functions, provide further support for this assumption. As mentioned in the description of experimental setup, the slit was made from two dull edge blades spaced 30 μm apart. Higher energy X ray would possibly see wider slit width considering its transmission through thin material. This effect could produce a strong tail of the image intensity distribution and leads to a deviation from the Gaussian distribution

function. The good fitting results of the image intensity distribution using Gaussian function illuminates that the transmission of X rays through the slit blades is negligible.

Another effect which could influence the effective slit width is the alignment of the slit with respect to the electron beam. During the installation of the Shanghai EBIT, the uprightness and the co-axiallity of the electron gun/drift tubes/beam position monitors were very carefully checked and the mount of the slit was also carefully done with the help of a plumb and a telescope. The misalignment was controlled under 1 mrad, which leads to around 1% increment of the FWHM. The effect has been taken into account in the final uncertainties and listed in Tables 1 to 3.

The pixel size of the CCD detector used in our experiments is not infinitely small, so the electrons produced by a photon hitting anywhere within a given pixel will be merged and converted to a count of this particular pixel. Hence, the image will be quantized in terms of pixels and distorted depending on the size of the pixel. Ray tracing simulations were performed both with and without the quantization effects. The results showed Gaussian distributions in both cases, but with a difference in FWHM. Figure 7 shows the ratios of the FWHM with quantization (the pixel size is set to be 13.5 μm, the same as that of the CCD used in our experiments) to that without quantization, against the electron beam size, σ. We defined this ratio as zoom ratio and could find it to exponentially decrease with σ increasing in Fig. 7 and the influence on the image width by quantization is less then 5% under our experimental conditions.

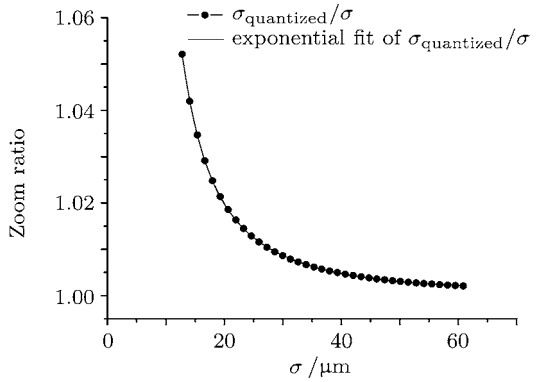

Fig. 7. A plot of the results obtained from ray tracing procedures. The zoom ratio is defined as the ratio of the FWHM with quantization over the FWHM without the quantization. Here σ relates to the width of the electron beam image FWHM and FWHM $= 2\sqrt{2\ln 2}\sigma$.

To calculate the density of the electron beam, we assume that the cross section of the beam is circular with a diameter equal to the FWHM of the two-dimensional radial Gaussian distribution. Then the current passing through this cross section is expressed as

$$\begin{aligned} I_{\rm FWHM} &= I \cdot \int_{-\rm FWHM}^{+\rm FWHM} {\rm d}x \int_{-\infty}^{+\infty} G_r(x,y){\rm d}y \qquad (2)\\ &= I \cdot 2\int_{0}^{+\rm FWHM} \frac{1}{\sigma\sqrt{2\pi}}\ \exp\left(-\frac{x^2}{2\sigma^2}\right){\rm d}x\\ &= 0.761I, \end{aligned}$$

where I is the total beam current. We could see only 76.1% of the total current passing this cross section. We then used this current to obtain the electron beam density, so as to avoid the overestimation of the beam density.

In order to make the analysis more convenient for future experiments, a computer program was written taking all the mentioned processes and effects into account. The program is available on request.

4. Results and discussion

Table 1 shows the diameters, the beam densities and the electron densities of the electron beam at 81 keV, with a current of 120 mA, 100 mA, and 80 mA. Table 2 shows the results at 50 keV with a current of 113 mA, 100 mA, and 80 mA separately. Table 3 shows the results for the 20 keV beam with a current of 80 mA and 60 mA separately and for a 100 keV beam of 100 mA. The results show that the diameter of the electron beam increases with current for a given electron beam energy, which means the beam density would not increase linearly with the current. The errors listed in the tables were obtained taking into account the uncertainties in determining image distance, object distance, silt width, slit alignment and the uncertainties of the fitted σ of the Gaussian distribution of the images recorded.

We believe that the width of the X-ray image from the ion cloud is a good approximation to the width of the electron beam for the reasons to be outlined below. The radial trapping potential in the central drift tube is around 50 V, hence a highly charged ion, W^{50+} for example, would experience a potential of 2.5 keV. The thermal energy of most trapped ions does not usually exceed this energy,[7−10] otherwise they would leave the trap. This means the velocity of such a trapped ion is below 10^7 mm$\cdot$s^{-1}. The X-ray images were formed mostly by the de-excitation photon emissions

through allowed electric dipole transitions which have lifetimes of 10^{-13} s or even shorter. Hence the maximum distance which ions could move after excitation and before de-excitation is around 10^{-3} μm. This is negligibly small compared with typical electron beam radius in an EBIT, which is several tens of μm. Also because of the thermal energy, the trapped ions are rotating all the times around the magnetic lines which are parallel to the electron beam. The rotation radius of W^{50+}, for example, is around five hundred μm under 3 T of magnetic field strength, which is typical for a cryogenic EBIT. The rotation would average out the distribution of the trapped ions inside the electron beam. So the image of the electron beam impact X-ray fluorescence of the ion cloud in an EBIT can be a good approximation of the electron beam.

Table 1. Widths and densities of the electron beams at beam energy of 81 keV, uncertainties are in parentheses.

I/mA†	FWHM/μm	Beam density /A·cm^{-2}	Density/cm^{-3}‡
120	$76.2(^{+4.3}_{-6.0})$§	$2.00(^{+0.32}_{-0.22})\times10^3$	7.1×10^{11}
100	$74.8(^{+4.4}_{-6.1})$	$1.72(^{+0.29}_{-0.20})\times10^3$	6.5×10^{11}
80	$68.5(^{+5.3}_{-7.0})$	$1.65(^{+0.35}_{-0.26})\times10^3$	6.8×10^{11}

† Electron beam current. ‡ Estimation of the density of electrons in the centre drift tube. Our results for the electron density are comparable to those found in Ref. [11]. § The unbalance of the uncertainty is caused by the effect of the nonperpendicularity of the slit.

Table 2. Widths and densities of the electron beams at beam energy of 50 keV, uncertainties are in parentheses.

I/mA†	FWHM /μm	Beam density /A·cm^{-2}	Density/cm^{-3}
113	$74.8(^{+4.4}_{-6.1})$	$1.96(^{+0.32}_{-0.23})\times10^3$	7.1×10^{11}
100	$72.8(^{+4.7}_{-6.4})$	$1.83(^{+0.33}_{-0.24})\times10^3$	6.9×10^{11}
80	$66.1(^{+5.9}_{-7.6})$	$1.77(^{+0.42}_{-0.32})\times10^3$	7.3×10^{11}

† The quantities are defined in Table 1.

Table 3. Widths and densities of the electron beams at beam energy of 20 keV and 100 keV, uncertainties are in parentheses.

E/keV†	I/mA	FWHM/μm	Beam density /A·cm^{-2}	Density/cm^{-3}
20	80	$68.1(^{+5.5}_{-7.3})$	$1.68(^{+0.35}_{-0.27})\times10^3$	1.3×10^{12}
20	60	$66.3(^{+5.7}_{-7.5})$	$1.32(^{+0.31}_{-0.23})\times10^3$	1.0×10^{12}
100	100	$75.5(^{+4.7}_{-6.5})$	$1.70(^{+0.29}_{-0.21})\times10^3$	6.5×10^{11}

† Electron beam energy. The other quantities are defined in Table 1.

There are at least two possible mechanisms which would lead larger widths to be measured if the part of the image containing all photons (including visible light up to X-ray) were used. The first mechanism is due to the fact that longer wavelength photons can be emitted either (a) by lower charge states and outer electron transitions or (b) from the decay of forbidden transitions in highly charged ions. Outer electron transitions in lower charged ions, as well as forbidden transitions in highly charged ions are both slower transitions which made it possible for ions to move farther before the photon decay occurs.[5] The second broadening mechanism is due to the diffraction by the 30-μm slit. By using only the X-ray image we do not need to consider broadening by diffraction as it would be on the order of 1.2 μm for 2 keV photons, which is the low energy limit in our setup. For higher energy photons, diffraction is smaller. For these reasons we choose to work in the X-ray range.

5. Conclusion

In this work, the electron beam profile at the Shanghai EBIT is studied under various beam conditions using a slit imaging technique. A numerical deconvolution method is developed to analyse and reconstruct the electron beam density distribution, through a slit imaging system. As a result of these studies, a removable flexible imaging system is developed, which is also possible for low magnification cases.

It is clear that such a system can provide important data on the electron beam radius and hence electron density. Such data are of great importance for atomic physics experiments aimed at determining cross sections for various processes and also at diagnosing the ion cloud plasma.

Acknowledgment

We would like to thank W. Hu, X. Zhang, W. Zhang, and S. Wu for their help during the experiments.

References

[1] Beiersdorfer P and Berkeley. 2008 *Can. J. Phys.* **86** 1
[2] Feng W T, Ma X W, Liu H P, Chen L F, Li B and Cao S P 2007 *Acta Phys. Sin.* **56** 3637 (in Chinese)
[3] Utter S B, Beiersdorfer P, Crespo L'opez-Urrutia J R and Widmann K 1999 *Nucl. Instrum. Method* A **428** 276
[4] Knapp D, Marrs R, Elliot S, Magee E and Zasadzinski R 1993 *Nucl. Instrum. Method* A **334** 305
[5] Crespo L'opez-Urrutia J R, Beiersdorfer P, Widmann K and Decaux V 2002 *Can. J. Phys.* **80** 1687

[6] Porto J V, Kink I and Gillaspy J D 2000 *Rev. Sci. Instrum.* **71** 3050

[7] Nakamura N, Faenov A Ya, Pikuz T A, Nojikawa E, Shiraishi H, Currell F J and Ohtani S 1999 *Rev. Sci. Instrum.* **70** 1658

[8] Beiersdorfer P, Osterheld A L, Decaux V and Widmann K 1996 *Phys. Rev. Lett.* **77** 5353

[9] Beiersdorfer P, Decaux V and Widmann K 1995 *Nucl. Instrum. Method* B **98** 566

[10] Beiersdorfer P, Decaux V, Elliott S R, Widmann K and Wong K 1995 *Rev. Sci. Instrum.* **66** 303

[11] Chen H, Beiersdorfer P, Heeter L A, Liedahl D A, Naranjo-Rivera K L, Träbert E, Gu M F and Lepson J K 2004 *The Astrophysical Journal* **611** 598